Structural Basis of Plasticity in Protein Tyrosine Phosphatase 1B Substrate Recognition[†,‡]

Mauro Sarmiento,[§,||] Yoram A. Puius,[§,||] Stefan W. Vetter,[§,⊥] Yen-Fang Keng,[⊥] Li Wu,[⊥] Yu Zhao,[⊥] David S. Lawrence,[§] Steven C. Almo,*[,§] and Zhong-Yin Zhang*[,§,⊥]

Departments of Biochemistry and Molecular Pharmacology, The Albert Einstein College of Medicine of Yeshiva University, 1300 Morris Park Avenue, Bronx, New York 10461

Received February 10, 2000; Revised Manuscript Received April 21, 2000

ABSTRACT: Protein tyrosine phosphatase 1B (PTP1B) displays a preference for peptides containing acidic as well as aromatic/aliphatic residues immediately NH_2-terminal to phosphotyrosine. The structure of PTP1B bound with DADEpYL-NH_2 ($EGFR^{988-993}$) offers a structural explanation for PTP1B's preference for acidic residues [Jia, Z., Barford, D., Flint, A. J., and Tonks, N. K. (1995) *Science 268*, 1754−1758]. We report here the crystal structures of PTP1B in complex with Ac-ELEFpYMDYE-NH_2 (PTP1B·Con) and Ac-DAD(Bpa)pYLIPQQG (PTP1B·Bpa) determined to 1.8 and 1.9 Å resolution, respectively. A structural analysis of PTP1B·Con and PTP1B·Bpa shows how aromatic/aliphatic residues at the −1 and −3 positions of peptide substrates are accommodated by PTP1B. A comparison of the structures of PTP1B·Con and PTP1B·Bpa with that of PTP1B·$EGFR^{988-993}$ reveals the structural basis for the plasticity of PTP1B substrate recognition. PTP1B is able to bind phosphopeptides by utilizing common interactions involving the aromatic ring and phosphate moiety of phosphotyrosine itself, two conserved hydrogen bonds between the Asp48 carboxylate side chain and the main chain nitrogens of the pTyr and residue 1, and a third between the main chain nitrogen of Arg47 and the main chain carbonyl of residue −2. The ability of PTP1B to accommodate both acidic and hydrophobic residues immediately NH_2-terminal to pTyr appears to be conferred upon PTP1B by a single residue, Arg47. Depending on the nature of the NH_2-terminal amino acids, the side chain of Arg47 can adopt one of two different conformations, generating two sets of distinct peptide binding surfaces. When an acidic residue is positioned at position −1, a preference for a second acidic residue is also observed at position −2. However, when a large hydrophobic group occupies position −1, Arg47 adopts a new conformation so that it can participate in hydrophobic interactions with both positions −1 and −3.

Protein tyrosine phosphatases (PTPases),[1] together with protein tyrosine kinases, control the tyrosine phosphorylation state in the cell, which is important for cellular activities such as growth, differentiation, motility, cell−cell interactions, metabolism, gene transcription, and the immune response (*1*, *2*). PTPases constitute a growing family of transmembrane (receptor-like) and intracellular enzymes that rival the protein tyrosine kinases in terms of structural diversity and complexity. Extensive biochemical and structural studies on PTPases during the past 10 years have led to a detailed understanding of the mechanism by which PTPases catalyze phosphate monoester hydrolysis (*3*, *4*). The exact functional roles of PTPases in cellular processes are currently under intensive investigation in numerous laboratories (*5*−*9*).

PTP1B is the first PTPase to be purified and characterized (*10*−*12*) and is the prototypical intracellular PTPase found in a wide variety of human tissues (*13*). PTP1B is capable of dephosphorylating a number of receptor tyrosine kinases, including the insulin receptor, the EGF receptor, and the PDGF receptor (*14*−*19*). Transient overexpression of PTP1B and a panel of receptor tyrosine kinases showed that PTP1B preferentially dephosphorylates the receptor precursors localized in the endoplasmic reticulum (*15*), which is in accord with the known cellular localization of PTP1B to the endoplasmic reticulum (*20*, *21*). Thus, the function of PTP1B is proposed to control the kinase function of nascent receptors during biosynthesis and transport to the cell surface (*15*). Such a mechanism may be critical in preventing the premature activation of the receptor tyrosine kinases in the

[†] This work was supported by NIH Grant GM55242. Z.-Y.Z. is a Sinsheimer Scholar and an Irma T. Hirschl Career Scientist. S.C.A. is also an Irma T. Hirschl Career Scientist. M.S. is supported by NIH Grant 5T32 GM 07491. Y.A.P. is supported by Medical Scientist Training Program Grant T32 GM07288 from the NIH.

[‡] The coordinates for the structures of PTP1B/C215S in complex with the consensus and Bpa-containing peptides have been deposited with the Protein Data Bank under accession numbers 1EEO and 1EEN, respectively.

* To whom correspondence should be addressed. S.C.A.: phone, (718) 430-2746; fax, (718) 430-8565; e-mail, almo@aecom.yu.edu. Z.-Y.Z.: phone, (718) 430-4288; fax, (718) 430-8922; e-mail, zyzhang@aecom.yu.edu.

[||] These two authors contributed equally to this work.

[§] Department of Biochemistry, The Albert Einstein College of Medicine of Yeshiva University.

[⊥] Department of Molecular Pharmacology, The Albert Einstein College of Medicine of Yeshiva University.

[1] Abbreviations: PTPase, protein tyrosine phosphatase; PTP1B, protein tyrosine phosphatase 1B; *p*NPP, *p*-nitrophenyl phosphate; Bpa, *p*-benzoylphenylalanine; pY, phosphotyrosine; EGFR, epidermal growth factor receptor; EDTA, ethylenediaminetetraacetic acid.

10.1021/bi000319w CCC: $19.00
Published on Web 06/23/2000

cell. For this mechanism to work, PTP1B must exhibit broad substrate specificity so that it can cleave the phosphoryl moiety from multiple and diverse autophosphorylation sites in receptor tyrosine kinases with high efficiency.

A further understanding of the specific functional roles that PTPases play in cellular signaling requires the identification of the physiological substrates for each member of the PTPase family and a detailed description of the structural features that control PTPase substrate specificity. Despite the remarkable progress in the identification and characterization of new PTPases and in the understanding of PTPase catalysis, the molecular basis by which PTPases distinguish and recognize the diverse substrates that they encounter in the cell remains elusive. This is partly because the physiological substrates for most PTPases remain unknown. Furthermore, since the physiological substrates for PTPases are phosphoproteins, even if the identity of the true physiological substrate is known, it remains a major obstacle to obtain quantities of specifically and stoichiometrically tyrosine-phosphorylated proteins required for detailed enzymological studies. Thus, the current approach for probing PTPase substrate specificity relies on the use of synthetic phosphotyrosine (pY)-containing peptides that correspond to the phosphorylated species found in vivo (*22*−*31*).

PTP1B displays a wide range of k_{cat}/K_m values for relatively short peptide substrates. The k_{cat}/K_m values for some of the peptide substrates approach the diffusion limit and are 3−4 orders of magnitude higher than that of pY alone, suggesting that residues flanking the pY moiety make significant contributions to high-affinity binding and catalysis. The kinetic analysis of many naturally occurring phosphopeptides identified the undecapeptide, EGFR$^{988-998}$ (epidermal growth factor receptor autophosphorylation site Tyr992, residues 988−998, DADEpYLIPQQG), as an excellent substrate for PTP1B (*25*, *26*). Alanine-scanning analysis of the EGFR$^{988-998}$ peptide revealed that PTP1B has a moderate preference for acidic residues at positions NH_2-terminal to pY, particularly at position −1 (*26*). However, other biochemical data indicate a preference for aromatic/aliphatic residues at position −1. For example, when the Glu(−1) residue in EGFR$^{988-998}$ is replaced with *p*-benzoylphenylalanine (Bpa), the resulting Bpa peptide Ac-DAD(Bpa)pYLIPQQG exhibits a k_{cat}/K_m similar to that of the parent peptide (Table 1; *32*). In addition, peptide substrates in which the −1 position is occupied by an aromatic (Neu$^{546-556}$, DNLYpYWDQNSS) or an aliphatic amino acid (p130Cas$^{258-269}$, Ac-PATDLpYQVPPGP-NH_2, and p130Cas$^{380-391}$, Ac-PLLDVpYDVPPSV-NH_2) also display kinetic parameters similar to that of the EGFR$^{988-998}$ peptide (Table 1). These data suggest that PTP1B can accommodate large aromatic/aliphatic residues as well as acidic side chains at position −1. Indeed, a preference for acidic (Asp and Glu), aromatic (Phe and Tyr), and aliphatic (Leu, Ile, Val, and Thr) residues at position −1 has also been observed using an "inverse alanine scanning" peptide library approach (*33*). The consensus peptide Ac-ELEFpYMDYE-NH_2 identified from this library contains a Phe at position −1 and is a potent substrate for PTP1B (Table 1).

Given the biochemical data, it may be tempting to speculate that PTP1B's ability to recognize such diverse peptide sequences results primarily from interactions between PTP1B and the peptide backbone and that interactions with the peptide side chains make little contribution to binding and catalysis. This is not the case, however, as the k_{cat}/K_m for AAAApYAAAA is ∼10-fold lower than those of the best peptides and specific substitutions in peptide substrates lead to significant decreases in k_{cat}/K_m (*26*, *33*). Furthermore, the crystal structure of the catalytically inactive mutant PTP1B (C215S) complexed with EGFR$^{988-993}$ (*34*) indicates specific ionic interactions between the acidic side chains at positions −1 and −2 of the substrate and the basic PTP1B residues Arg47 and Lys41. This complex provides a structural basis for PTP1B's preference for acidic peptides; however, it does not explain how PTP1B can equally accommodate aromatic/aliphatic peptides. The ionic interactions observed between the basic residues of the enzyme and acidic residues of the EGFR peptide would seem to preclude an equal preference for aromatic/aliphatic amino acids at the same position, suggesting that additional determinants for peptide substrate recognition by PTP1B must exist.

Table 1: Kinetic Constants for the Hydrolysis of pTyr-Containing Peptides by PTP1B[a]

substrate		k_{cat}/K_m ($\times 10^{-7}$ M^{-1} s^{-1})
DADEpYLIPQQG[b]	EGFR$^{988-998}$	2.88 ± 0.24
DADEpYL-NH_2[b]	EGFR$^{988-993}$	2.24 ± 0.18
DNLYpYWDQNSS[c]	Neu$^{546-556}$	1.64 ± 0.10
Ac-PATDLpYQVPPGP-NH_2[d]	p130Cas$^{258-269}$	2.48 ± 0.09
Ac-PLLDVpYDVPPSV-NH_2[d]	p130Cas$^{380-391}$	2.10 ± 0.14
DAD**Bpa**pYLIPQQG[e]	Bpa peptide	2.10 ± 0.11
Ac-ELEFpYMDYE-NH_2[f]	consensus peptide	2.20 ± 0.05

[a] All measurements were performed at pH 6.6 and 30 °C except the consensus peptide, which was performed at pH 7.0 and 30 °C. k_{cat} and K_m values have been measured for EGFR$^{988-998}$, EGFR$^{988-993}$, Neu$^{546-556}$, the Bpa peptide, and the consensus peptide (*25*, *27*, *32*, *33*). Results from these studies and many others show that the k_{cat} values of peptide substrates are similar for PTP1B. This is because the rate-limiting step corresponds to the hydrolysis of the phosphoenzyme intermediate. In the current work, only k_{cat}/K_m values have been measured for p130Cas$^{258-269}$ and p130Cas$^{380-391}$, assuming that they will display similar k_{cat} values as well. [b] From ref *27*. [c] From ref *25*. [d] This study. [e] From ref *32*. [f] From ref *33*.

Since the available PTP1B·EGFR$^{988-993}$ structure does not provide a satisfactory structural explanation for the recognition of Ac-DAD(Bpa)pYLIPQQG and Ac-ELEFpYMDYE-NH_2 by PTP1B, we have determined the X-ray structures of PTP1B bound with these two peptides. The crystal structures of the catalytically inactive C215S mutant of PTP1B bound with the consensus peptide, Ac-ELEFpYMDYE-NH_2 (PTP1B·Con), and Ac-DAD(Bpa)pYLIPQQG (PTP1B·Bpa), show how these two peptides are accommodated within the peptide-binding surface of PTP1B. A comparison of the structures of PTP1B·Con and PTP1B·Bpa with that of PTP1B·EGFR$^{988-993}$ reveals the structural basis for the ability of PTP1B to bind peptides of diverse sequences. The characterization and detailed understanding of PTP1B substrate recognition may assist in the development of potent PTP1B specific inhibitors and may contribute to the effort in the identification of in vivo substrates of PTP1B.

EXPERIMENTAL PROCEDURES

Materials. The phosphopeptides EGFR$^{988-998}$ DADEpYLIPQQG, Bpa peptide Ac-DAD(Bpa)pYLIPPQG, consensus peptide Ac-ELEFpYMDYE-NH_2, p130Cas$^{258-269}$ Ac-

PATDLpYQVPPGP-NH_2, and p130Cas$^{380-391}$ Ac-PLLD-VpYDVPPSV-NH_2 were synthesized, purified, and characterized as described previously (*25*, *32*, *33*). The C215S mutant form of PTP1B was purified as described previously (*35*).

Determination of Kinetic Constants. All assays were performed at 30 °C in 50 mM 3,3-dimethylglutarate, 1 mM EDTA, 0.15 M ionic strength buffer (pH 7). A continuous spectrophotometric assay previously described (*31*) was employed to determine k_{cat}/K_m for the pY-containing peptides. The dephosphorylation reaction was monitored by an increase in absorbance at 282 nm (*25*), measured on a Perkin-Elmer Lambda 14 spectrophotometer equipped with a water-jacketed cell holder, permitting maintenance of the reaction mixture at the desired temperature (30 °C).

Cocrystallization of PTP1B/C215S with Peptide Substrates. Crystals were grown by hanging-drop vapor diffusion at 4 °C using slight modifications of methods previously described (*34*, *35*). Stock solutions of PTP1B/C215S (10 mg/mL) in 100 mM MES (pH 6.5), 25 mM NaCl, 0.2 mM EDTA, and 3.0 mM DTT were prepared with either 5 mM Ac-DAD(Bpa)pYLIPQQG peptide or 150 μM Ac-ELEFpYMDYE-NH_2 peptide. In each well, a 5 μL drop of each stock solution was mixed with an equal volume of the precipitating solution [0.1 M Hepes (pH 7.0−7.5), 0.2 M magnesium acetate, and 12−20% (w/v) polyethylene glycol 8000 (Fluka)] and the mixture equilibrated against 1 mL of the precipitating solution.

Data Collection and Processing. For the complex between PTP1B/C215S and Ac-ELEFpYMDYE-NH_2, a single crystal was transferred at 4 °C directly into a cryoprotectant solution that contained crystallization buffer, 20% (v/v) glycerol, and 150 μM peptide. The crystal was transferred to a loop and cooled in nitrogen gas. A wavelength of 0.9795 Å was used to collect 363 frames of 0.5° each using an ADSC Quantum 4 CCD detector at beamline X9B at the National Synchrotron Light Source (Brookhaven National Laboratory, Upton, NY).

A single crystal of the complex between PTP1B/C215S and Ac-DAD(Bpa)pYLIPQQG was transferred at 4 °C in increments of 5% glycerol concentration (2 min interval at each concentration) to a final cryoprotectant solution that contained crystallization buffer, 25% (v/v) glycerol, and 5 mM peptide. The crystal was transferred to a loop and flash-cooled in a stream of nitrogen gas at 140 K. A wavelength of 1.20 Å was used to collect 150 frames of 1° each on Fuji image plates utilizing the custom-built apparatus described previously (*35*) at beamline X9B at the National Synchrotron Light Source (Brookhaven National Laboratory).

All data were reduced with the HKL package of programs (*36*) using an I/σ_I cutoff of 0. Data reduction statistics are shown in Table 2. Analysis of the data with DATAMAN (*37*) indicated significant anisotropy in the data set of the complex with Ac-DAD(Bpa)pYLIPQQG, where the intensity fell off significantly more slowly along the *l* axis.

Structure Solution. Both structures were determined by molecular replacement using the program AMoRe (*38*). The starting model used in both cases was the structure of PTP1B/C215S in the presence of 53 mM pTyr (*35*), but with solvent molecules, ligands, and loop residues 179−189 deleted. A single outstanding peak with a correlation coefficient greater than twice the height of the next highest peak was observed in the cross-rotation search of both structures, and both translation functions exhibited a major peak with a correlation coefficient 1.6−1.7 times higher than that of the second highest peak (Table 2).

The refinement of both structures using the programs X-PLOR (*39*) and CNS 0.9 (*40*) proceeded essentially identically. Rigid-body refinement using 8.0−3.0 Å data was followed by 4000 K simulated annealing against 25.0−2.5 Å data with the incorporation of an isotropic bulk solvent model (*41*). Density for the loop (residues 179−189) and peptide was evident immediately after the first round of refinement. Subsequent rounds of refinement consisted of simulated annealing, positional refinement, and temperature factor refinement using 25.0−1.9 Å data for the Ac-DAD(Bpa)pYLIPQQG complex and 25.0−1.8 Å data for the Ac-ELEFpYMDYE-NH_2 complex. Global anisotropic temperature factors B_{11}, B_{22}, and B_{33} were refined at the beginning of each round of refinement for both data sets. Model building was performed using the program O (*42*). Simulated annealing OMIT maps (*43*), R_{free} values (*44*), PROCHECK (*45*), and WHAT IF (*46*) were employed to ensure correct model building and stereochemistry.

The Ac-ELEFpYMDYE-NH_2 complex included residues 2−298 of the enzyme, peptide residues corresponding to LEFpYMDYE, 226 water molecules, and one magnesium ion. The final model of the complex with Ac-DAD(Bpa)-pYLIPQQG consisted of residues 1−299 of PTP1B/C215S, peptide residues corresponding to AD(Bpa)pYLIP, 300 water molecules, one magnesium ion, and two acetate ions. Final refinement statistics are shown in Table 2.

RESULTS

The crystal structure of PTP1B/C215S in complex with the hexapeptide DADEpYL-NH_2 (PTP1B·EGFR$^{988-993}$) shows that Arg47 plays an important role in interacting with acidic amino acids at position −1 (*34*). Results from NMR and molecular dynamics studies of DADE(F_2Pmp)L (F_2Pmp, phosphonodifluoromethylphenylalanine) bound to PTP1B (*47*) are in agreement with the crystal structure. These observations offer a structural explanation for the preference of PTP1B for acidic residues NH_2-terminal to pY (*25*, *28*).

However, there are considerable data in the literature suggesting that PTP1B is somewhat promiscuous in its substrate preference as it dephosphorylates a wide variety of proteins and peptide substrates (*25*, *28*, *33*, *48*). For example, PTP1B hydrolyzes several unrelated pY-containing peptides with almost equal efficiency as the EGFR peptides (Table 1). It appears that, in addition to acidic residues, both aromatic (F, Y, or Bpa) and aliphatic (V or L) amino acids can also occupy position −1 in efficient peptide substrates (*33*). Furthermore, a selection for aromatic and aliphatic residues, in addition to the general preference for acidic residues at position −1, has also been observed in affinity selections from targeted peptide libraries containing non-hydrolyzable pY mimics (F_2Pmp or malonyltyrosine) using the EGF receptor peptide DADEpYL as a template (*49*, *50*). These results suggest that the −1 binding site possesses a remarkable degree of flexibility so that residues with drastically different structures can be accommodated. The crystal structures of PTP1B in complex with the consensus peptide derived from the inverse alanine scanning approach,

Table 2: Crystal, Data Collection, Molecular Replacement, and Refinement Statistics

	PTP1B/C215S and Ac-ELEFpYMDYE-NH_2	PTP1B/C215S and Ac-DAD(Bpa)pYLIPQQG
crystal parameters		
space group	$P2_12_12_1$	$P2_12_12_1$
cell constants	$a = 52.58$ Å, $b = 82.05$ Å, $c = 88.54$ Å, and $\alpha = \beta = \gamma = 90°$	$a = 66.35$ Å, $b = 72.54$ Å, $c = 88.47$ Å, and $\alpha = \beta = \gamma = 90°$
data collection		
resolution range (Å)	25.0−1.80 (1.86−1.80)[a]	24.1−1.90 (1.97−1.90)
no. of measurements	180537	160542
no. of unique reflections ($I > 0\sigma$)	34694 (2629)	32272 (2160)
completeness (%)	95.4 (73.5)	93.3 (63.7)
R_{merge} (%)[b]	3.6 (8.6)	3.5 (13.1)
mean I/σ of merged data	30.3 (14.2)	20.7 (4.8)
wavelength (Å)	0.9795	1.20
molecular replacement statistics[c]		
resolution range (Å)	25.0−4.0	25.0−4.0
rotation function peak (σ)	12.5	12.1
correlation coefficient (%)	22.0	19.4
translation function peak (σ)	12.5	13.7
correlation coefficient	59.5	61.8
R factor	39.6	37.4
rigid-body refinement		
correlation coefficient	61.2	60.6
R factor	38.7	37.6
refinement statistics		
resolution range (Å)	24−1.8 (1.86−1.80)	20−1.9 (1.97−1.90)
no. of reflections used for refinement	34624 (2579)	32081 (2070)
no. of reflections used for R_{free}	1074 (92)	1641 (115)
crystallographic R factor[d]	18.3 (21.8)	18.8 (28.2)
R_{free}[e]	21.2 (22.5)	21.7 (36.4)
rms bond length deviation (Å)[f]	0.007	0.010
rms bond angle deviation (deg)[f]	1.3	1.4
no. of atoms		
PTP1B/C215S	2427	2442
peptide	82	71
water	226	300
Mg^{2+}	1	1
acetate ions	0	8
all atoms	2736	2821
overall anisotropic temp factors (Å^2)		
B_{11}	−2.55	10.60
B_{22}	6.36	3.70
B_{33}	−3.81	−14.30
average temp factors (Å^2)		
PTP1B/C215S	17.7	33.0
peptide	19.1	37.4
water	29.5	44.7
Mg^{2+}	59.4	33.8
acetate	−	44.1
all atoms	18.7	34.3
Cα rmsd of residues 2−298 (Å)[g] when compared to		
PTP1B·$EGFR^{988-993}$	0.48	0.45
PTP1B·Con	−	0.33
PTP1B·Bpa	0.33	−

[a] Numbers in parentheses refer to the highest-resolution shell of data. [b] $R_{merge} = \Sigma_{hkl}\Sigma_n|\langle I(hkl)\rangle - I_n(hkl)|/\Sigma_{hkl}\Sigma_n I_n(hkl)$, where $I_n(hkl)$ and $\langle I(hkl)\rangle$ are the nth and mean measurements of the intensity of reflection hkl. [c] From AMoRe (*38*). [d] $R_{cryst} = \Sigma_{hkl}|F_o - F_c|/\Sigma_{hkl}F_o$, where F_o and F_c are the observed and calculated structure factor amplitudes, respectively, for all reflections hkl used in refinement. [e] R_{free} is R_{cryst} calculated for the data which were sequestered and not used in refinement (*44*). [f] As calculated by CNS (*40*) using the stereochemical criteria of Engh and Huber (*52*). [g] As calculated with ProFit (*53*).

Ac-ELEFpYMDYE-NH_2 (PTP1B·Con), and the $EGFR^{988-998}$ peptide in which the Glu(−1) is substituted with Bpa, Ac-DAD(Bpa)pYLIPQQG (PTP1B·Bpa), provide a structural mechanism for this plasticity.

Structures of PTP1B·Con and PTP1B·Bpa. The final model for the PTP1B·Con structure included protein residues 2−298 and all residues in the consensus peptide except for the extreme NH_2-terminal Glu. The structure was refined to an R factor of 0.183 ($R_{free} = 0.212$) for data to 1.8 Å resolution. The PTP1B·Bpa model was refined to an R factor of 0.188 ($R_{free} = 0.217$) for data to 1.9 Å resolution, which included protein residues 1−299 and the Bpa peptide residues from −3 to 3. The final refinement statistics are summarized in Table 2. Residues of the phosphopeptides bound to PTP1B were fitted unambiguously to well-defined electron density (Figure 1), although that for the residue at position −4 of the consensus peptide and those for positions −4, 4, 5, and 6 of the Bpa peptide were not visible.

The overall structures of PTP1B in the two crystal forms described here are quite similar to each other and to the $EGFR^{988-993}$ complex, as demonstrated by Cα rmsd values of 0.3−0.5 Å (Table 2). A comparison between the two

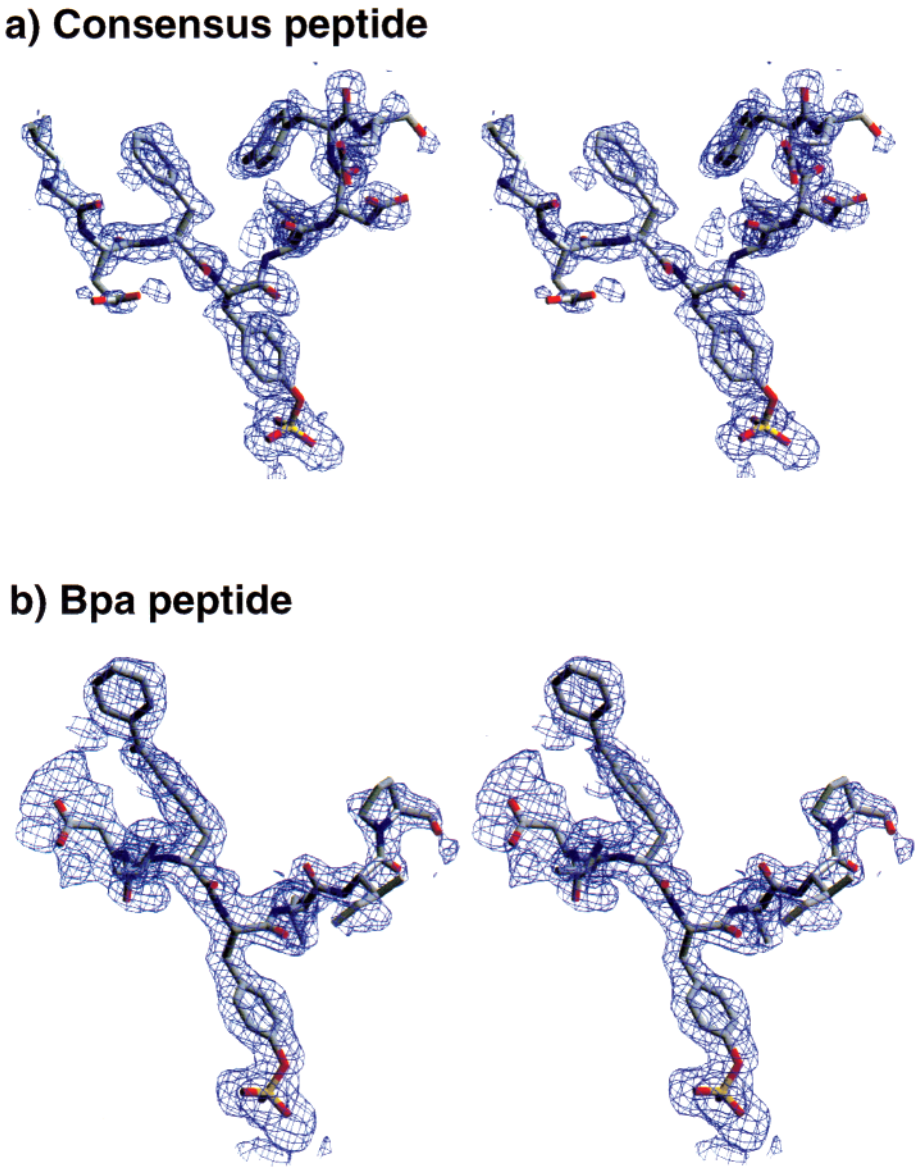

FIGURE 1: Stereoview of 4000 K simulated annealing OMIT density of (a) the consensus peptide and (b) the Bpa peptide bound to PTP1B/C215S. The density is an $F_o - F_c$ map contoured at 0.9σ. This figure was generated using SETOR (*51*).

PTP1B·peptide complexes and the ligand free form of PTP1B (*54*) showed that the overall protein structures are similar, with significant conformational differences confined to the active site upon ligand binding. In both cases, substrate binding induces the closure of the WPD loop (encompassing residues 179−189), which brings the general acid Asp181 in proximity to the ester oxygen in the substrate for efficient catalysis (*4*). Similar closed WPD loop conformations have also been observed in the oxyanion-bound *Yersinina* PTPase (*55*) and the pTyr- and DADEpYL-bound PTP1B structures (*34*, *35*).

Mode of Peptide Binding in PTP1B·Con and PTP1B·Bpa. The bound peptides in the two structures have the same NH_2- to COOH-terminal orientations, similar to that observed for DADEpYL-NH_2 in the PTP1B·EGFR$^{988-993}$ structure (Figure 2). The backbones of all three peptides are approximately in an extended β-strand conformation, with some deviations toward the terminal residues (Figure 2 and Table 3). The position and environment of the pTyr residues of all three peptides are similar, with the phosphate moiety and the phenyl ring of the pTyr residue participating in hydrophobic and electrostatic interactions nearly identical to those observed in other PTP1B·substrate complexes (*34*, *35*). The terminal nonbridge phosphate oxygens form an extensive array of hydrogen bonds with the main chain nitrogens of the phosphate-binding loop (residues 215−221) and the guanidinium side chain of Arg221 (Figure 3). The phenyl ring of the pTyr residue is effectively buried within an active site cavity, formed by the nonpolar side chains of Ala217 and Ile219 of the phosphate-binding loop, Phe182 of the WPD loop, and Tyr46, Val49, and Gln262 (Figure 3).

Specific polar interactions between the enzyme and the peptide backbone stabilize the binding interface in both the PTP1B·Con and PTP1B·Bpa structures in a manner identical to that observed in the PTP1B·EGFR$^{988-993}$ complex (*34*). Most notably, Asp48 forms two hydrogen bonds to the main chain nitrogens of the pTyr and position 1 residues in both PTP1B·Con and PTP1B·Bpa structures (Figures 3 and 4). In addition, the main chain nitrogen of Arg47 forms hydrogen bonds with the main chain carbonyl of Glu(−2) in the consensus peptide and with the main chain carbonyl of Asp(−2) in the Bpa peptide (Figures 3 and 4).

Table 3: Torsion Angles for Selected Residues in Peptide Complexes of PTP1B/C215S

	EGFR hexamer				consensus peptide				Bpa peptide			
position	residue	ϕ	ψ	χ_1	residue	ϕ	ψ	χ_1	residue	ϕ	ψ	χ_1
peptide residue												
P−4	Asp	–	−94	−116								
P−3	Ala	5	−67	–	Leu	–	140	−60	Ala	–	−29	–
P−2	Asp	−25	−38	−117	Glu	−105	132	−151	Asp	−80	−16	−82
P−1	Glu	−91	146	45	Phe	−123	139	−62	Bpa	−120	135	−60
pY	pTyr	−114	−39	178	pTyr	−84	−40	179	pTyr	−98	−35	180
P1	Leu	−66	–	−93	Met	−84	168	−50	Leu	−69	135	−53
P2					Asp	−99	129	172	Ile	−96	124	−82
P3					Tyr	−119	12	−59	Pro	−56	–	29
P4					Glu	−93	–	−78				
PTP1B residue												
47	Arg	−59	−38	−173	Arg	−70	−22	−64	Arg	−69	−24	−58

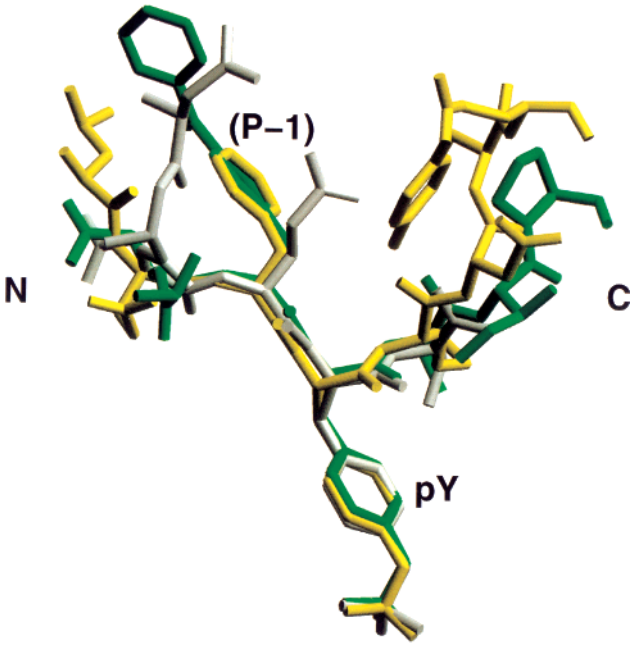

FIGURE 2: Superposition of the refined coordinates of the EGFR$^{988-993}$ peptide (gray), the consensus peptide (yellow), and the Bpa peptide (green). Superposition was performed with ProFit version 1.6 (*53*). This figure was generated using SETOR (*51*).

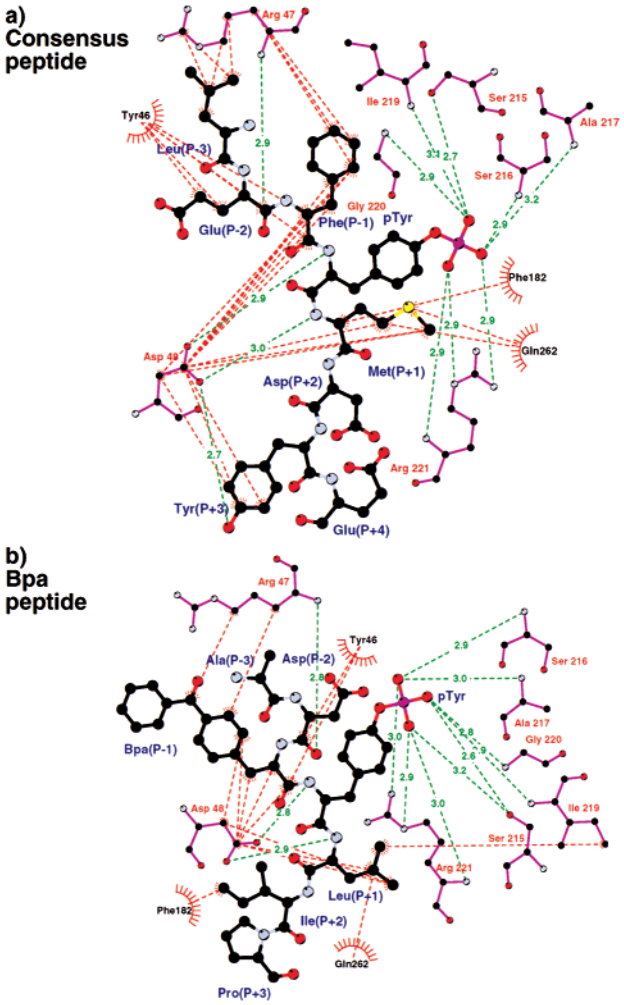

FIGURE 3: Schematic representation of the interactions between PTP1B/C215S with (a) the consensus peptide and (b) the Bpa peptide. Green dotted lines represent hydrogen bonds or electrostatic interactions, and red dotted lines represent hydrophobic interactions. Atom colors are as follows: carbon, black; nitrogen, blue; oxygen, red; sulfur, yellow; and phosphorus, purple. Distances shown are in angstroms. This figure was generated using LIGPLOT (*56*).

In both peptide-bound structures, specific interactions between peptide side chains and PTP1B are also observed. The bulky aromatic residues at position −1, Phe and Bpa in the PTP1B·Con and PTP1B·Bpa structures, respectively, occupy a largely hydrophobic patch formed by the aliphatic portions (i.e., methylene carbons) of the side chains of Arg47 and Asp48 (Figures 3 and 4), so that the proximal aromatic ring of Bpa and the ring of Phe are essentially superimposable (Figures 2 and 5). Leu(−3) of the consensus peptide makes a distinct van der Waals contact with the distal portion of the Arg47 side chain (Figures 3 and 4). At position 1, the Met of the consensus peptide and the Leu of the Bpa peptide reside in a largely hydrophobic pocket formed by the aliphatic side chains of Asp48, Val49, Ile219, and Gln262 (Figure 3). Additionally, the phenolic oxygen of the Tyr(3) residue in the PTP1B·Con structure participates in a hydrogen bonding interaction with the carboxylic side chain of Asp48.

Since the extended conformation of the peptide ligand directs side chains of adjacent residues in opposite directions, the carboxylic side chains of Glu(−2), Asp(2), and Glu(4) in the consensus peptide are pointed away from the enzyme. Asp(−2) and Ile(2) of the Bpa peptide also do not form any obvious interactions with the enzyme. Because the remaining peptide residues [Glu(−4) in the consensus peptide, and Asp(−4), Gln(4), Gln(5), and Gly(6) of the Bpa peptide] cannot be observed in the structures, additional interactions with these residues, if present, are likely to be weak.

DISCUSSION

A comparison of the PTP1B·Con and PTP1B·Bpa structures with the existing PTP1B·EGFR$^{988-993}$ structure reveals peptide sequence specific conformational changes in PTP1B and certain conserved structural characteristics which remain constant regardless of the sequence of the bound peptide. Localized conformational changes in PTP1B as well as differences in the secondary structure of the bound peptides (especially at the extreme NH_2-terminal positions) are also seen between the PTP1B·EGFR$^{988-993}$ structure and the PTP1B·Con and the PTP1B·Bpa structures. The conserved mode of interactions between the peptides and PTP1B and the unique peptide sequence specific conformational changes in PTP1B provide a structural basis for the observed plasticity in PTP1B substrate recognition.

Common Mode of Interaction. In all three structures, the bound peptide is similarly oriented (Figure 2), maintaining the same NH_2- to COOH-terminal direction relative to the protein surface. In addition, the backbones of certain positionally equivalent residues are in similar conformations in all three bound peptides. All three structures maintain two conserved hydrogen bonds between the Asp48 carboxylate side chain and the main chain nitrogens of the pTyr and residue 1, and a third between the main chain nitrogen of Arg47 and the main chain carbonyl of residue −2 (Figures 3 and 4). Consequently, the peptide backbones of residues from positions −1 to 1 in all three structures adopt a twisted β-strand conformation (Figure 2). This ensures that the pTyr is bound to PTP1B in an identical manner, regardless of the specific sequence adjacent to it.

Since Asp48 (or Asn) is conserved among all PTPases (*57*),[2] and its interactions with pTyr and residue 1 are conserved in all known crystal structures, Asp48 may be the primary and common determinant of the overall peptide orientation, and of the conformation of residues −1 to 1 (*34*, *57*). Indeed, the D48A mutation of PTP1B does not show any adverse effects on the hydrolysis of *p*-nitrophenyl phosphate, which lacks the corresponding main chain nitrogens. In contrast, when the EGFR$^{988-998}$ peptide is used as a substrate, the D48A mutant exhibits a 22-fold decrease in k_{cat}/K_m (*57*), consistent with the loss of two hydrogen bonds to the main chain nitrogens at the pTyr and position 1 residues. Interestingly, the D48A mutation has little effect on the hydrolysis of the phosphoenzyme intermediate (E−P), since the tyrosyl peptide with which the side chain of Asp48 interacts with is no longer present in the active site during E−P hydrolysis (*57*). These kinetic results are consistent with the structural data and suggest that Asp48 plays an important role in positioning the peptide substrates in an optimal conformation for peptide binding and/or the initial nucleophilic attack by the active site Cys residue.

Arg47 Is the Major Determinant for the Plasticity of Recognition for Amino Acids NH_2-Terminal to pTyr. The guanidinium group of Arg47 in the PTP1B·EGFR$^{988-993}$ structure is engaged in favorable electrostatic interactions with the side chains of Glu(−1) and Asp(−2) (Figure 4a).

[2] It should be noted that there are a few PTPases in which residues other than Asp or Asn have been found at this position, most notably, the cytoplasmic EC−PTP and LC−PTP, and the receptor-like PTPases, PTPψ, IA-2, and IA-2β (*57*). However, it is not clear whether these proteins are active tyrosine phosphatases.

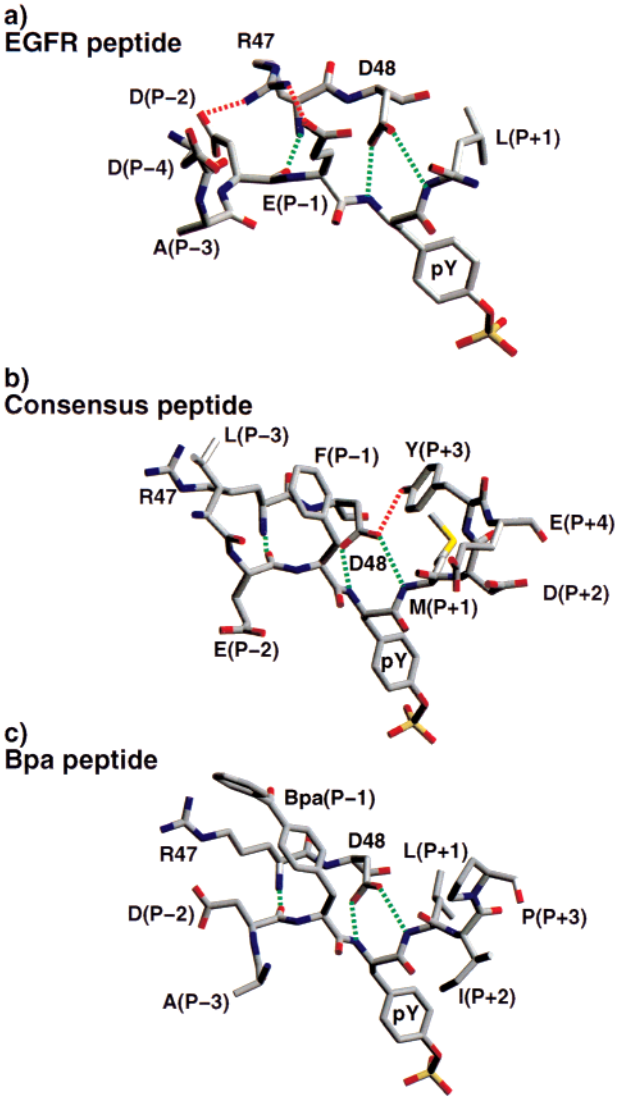

FIGURE 4: Side chain interactions between PTP1B/C215S and (a) EGFR$^{988-993}$, (b) the consensus peptide, and (c) the Bpa peptide. Green dashed lines represent hydrogen bonds conserved in all three complexes. Red dashed lines represent peptide specific hydrogen bonds. Note the different conformation of Arg47 in the consensus and Bpa peptide complexes as compared with that in the EGFR peptide complex. Distances shown are in angstroms. Atom colors are as follows: carbon, gray; nitrogen, blue; oxygen, red; and sulfur and phosphorus, yellow. This figure was generated using SETOR (*51*).

In this structure, the side chain of Arg47 also forms a long hydrogen bond with the main chain carbonyl of Asp(−4) (*34*). In the PTP1B·Con and PTP1B·Bpa structures, the bulky aromatic moieties at the −1 position, Phe and Bpa, respectively, induce a repositioning of the Arg47 side chain, highlighted by a change in the χ_1 angle of ∼120° (Table 3) and a 7 Å shift of the guanidinium carbon from the position observed in the PTP1B·EGFR$^{988-993}$ structure (Figure 5). This shift prevents the potential interactions between Arg47 and the residue at the −4 position in the PTP1B·Con and PTP1B·Bpa structures, as Arg47 now adopts a different side chain conformation. Since the position −4 residue is not visible in the PTP1B·Con and the PTP1B·Bpa structures, it is most likely not participating in any interactions with PTP1B.

The shift in the position of the Arg47 side chain enables PTP1B to accommodate aromatic residues at position −1.

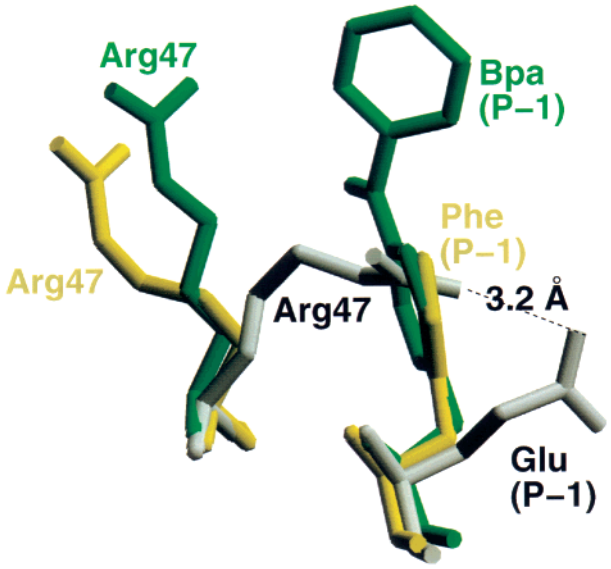

FIGURE 5: Superposition of the refined coordinates of Arg47 and the −1 residues of the EGFR$^{988-993}$ peptide (gray), the consensus peptide (yellow), and the Bpa peptide (green). This figure was generated using SETOR (*51*).

In the PTP1B·Con and PTP1B·Bpa structures, the aromatic side chain of Phe and the proximal ring of Bpa at position −1 contact the aliphatic portions of the side chains of Arg47 and Asp48 (Figures 3 and 4b,c). The placement of Arg47 in the PTP1B·Con structure also creates a unique hydrophobic contact with the Leu(−3) of the consensus peptide (Figure 4b) not present in the PTP1B·EGFR$^{988-993}$ or the PTP1B·Bpa complex. In short, the movement of Arg47 generates an altered binding mode for the NH_2-terminal residues, which is electrostatically and topologically distinct from that seen in the PTP1B·EGFR$^{988-993}$ structure. Consistent with previous biochemical data, model building based on the PTP1B·Con structure shows that Ile, Leu, Thr, and Val can all be effectively accommodated at position −1 without steric interference, as can Leu and Gln at position −3.

We propose that the conformation of Arg47 serves as the major determinant that allows for the accommodation of two types of peptide structures. When an acidic residue is positioned at position −1, as in the PTP1B·EGFR$^{988-993}$ structure, a preference for a second acidic residue is observed at position −2. However, when a large hydrophobic group occupies position −1, Arg47 adopts a new conformation so that it can participate in hydrophobic interactions with both positions −1 and −3.

To further substantiate the direct involvement of Arg47 in two distinct peptide binding modes, we measured the k_{cat}/K_m, the substrate specificity constant, for wild-type PTP1B and the R47E mutant using DADEpYLIPQQG (EGFR$^{988-998}$), Ac-ELEFpYMDYE-NH_2 (the consensus peptide), and the all-Ala peptide, Ac-AAAApYAAAA-NH_2. The observation that the k_{cat}/K_m values for the all-Ala peptide are similar for the wild type and the R47E mutant PTP1B further supports the notion that the side chain of Arg47 is primarily involved in side chain−side chain interactions with the substrates (Table 4). The finding that the all-Ala peptide is only ~10-fold less efficient than the EGFR$^{988-998}$ and the consensus peptides is in accord with the observation that the major interactions between PTP1B and peptide substrates involve the pTyr itself and the peptide backbone (ref *34* and this study). The Glu47 side chain retains most of the Arg47 atoms involved in the hydrophobic interaction with residue −1 of the consensus peptide, but lacks the guanidinium group which participates in ionic interactions with the NH_2-terminal acidic side chains of the EGFR$^{988-998}$ peptide. Thus, the R47E mutant would be expected to accommodate aromatic amino acids more easily than acidic residues at position −1, which is borne out by the finding that the R47E mutant exhibits a 7.9-fold decrease in k_{cat}/K_m for the EGFR$^{988-998}$ peptide but only a 2.7-fold decrease for the consensus peptide in comparison to wild-type PTP1B (Table 4). The slight decrease in k_{cat}/K_m for the R47E-catalyzed hydrolysis of the consensus peptide may be due to the lack of interaction between Glu47 and the side chain of Leu at position −3 (Figure 3a). Collectively, these results are consistent with the ability of Arg47 to interact with both acidic and hydrophobic residues.

Table 4: Kinetic Constants for the Hydrolysis of pTyr-Containing Peptides by PTP1B and PTP1B/R47E at pH 7.0 and 30 °C[a]

substrate	PTP1B k_{cat}/K_m ($\times 10^{-7}$ M^{-1} s^{-1})	PTP1B/R47E k_{cat}/K_m ($\times 10^{-7}$ M^{-1} s^{-1})
DADEpYLIPQQG	1.10 ± 0.04	0.14 ± 0.0005
Ac-ELEFpYMDYE-NH_2	2.20 ± 0.05	0.82 ± 0.01
Ac-AAAApYAAAA-NH_2	0.15 ± 0.0002	0.12 ± 0.0005

[a] The k_{cat} values for PTP1B and the R47E mutant with EGFR$^{988-998}$ are similar, and the decrease in k_{cat}/K_m is attributed to an increase in K_m (*57*). Only k_{cat}/K_m values have been measured for the consensus and the all-Ala peptides, assuming that PTP1B and the R47E mutant hydrolyze them with similar k_{cat} values and the changes in k_{cat}/K_m reflect variations in K_m.

Conclusions and Implications. Biochemical data summarized in this paper show that PTP1B possesses a rather relaxed specificity, capable of hydrolyzing peptide substrates with diverse sequence variations. The current structural analysis of PTP1B·Con and PTP1B·Bpa shows how PTP1B is able to accommodate hydrophobic residues at position −1 of peptide substrates. A comparison of the structures of PTP1B·Con and PTP1B·Bpa with that of PTP1B·EGFR$^{988-993}$ reveals the structural basis for the plasticity of PTP1B substrate recognition. The dominant interactions involve pTyr itself and the hydrogen bonds between peptide main chain atoms and the protein. The ability to accommodate both acidic and hydrophobic residues immediately NH_2-terminal to pTyr appears to be conferred upon PTP1B by a single residue, Arg47. Depending on the nature of the NH_2-terminal amino acids, the side chain of Arg47 can adopt two different conformations, generating two sets of distinct peptide binding surfaces. The ability of PTP1B to recognize common substrate features and to generate altered binding surfaces is central to its function as a broad specificity PTPase. Importantly, the unique topology and electrostatic potential associated with PTP1B plasticity should assist in the design of PTP1B specific inhibitors. Since mice lacking functional PTP1B exhibit increased sensitivity toward insulin and are resistant to obesity (*19*), specific inhibition of PTP1B may be therapeutically beneficial in the treatment of type II diabetes mellitus, insulin resistance, and obesity.

ACKNOWLEDGMENT

We thank Dr. Denise Rozwarski for collecting the consensus peptide data and Mr. Michael Sullivan for

assistance in collecting the Bpa peptide data. We also thank Dan McCain for helpful comments on the manuscript. Construction and operation of Beamline X9B is supported by National Center for Research Resource Grant RR01633 from the Department of Energy.

REFERENCES

1. Hunter, T. (1995) *Cell 80*, 225−236.
2. Tonks, N. K., and Neel, B. G. (1996) *Cell 87*, 365−368.
3. Barford, D., Das, A. K., and Egloff, M. P. (1998) *Annu. Rev. Biophys. Biomol. Struct. 27*, 133−164.
4. Zhang, Z.-Y. (1998) *CRC Crit. Rev. Biochem. Mol. Biol. 33*, 1−52.
5. Walton, K. M., and Dixon, J. E. (1993) *Annu. Rev. Biochem. 62*, 101−120.
6. Streuli, M. (1996) *Curr. Opin. Cell Biol. 8*, 182−188.
7. Neel, B. G., and Tonks, N. K. (1997) *Curr. Opin. Cell Biol. 9*, 193−204.
8. Chernoff, J. (1999) *J. Cell. Physiol. 180*, 173−181.
9. den Hertog, J. (1999) *Mech. Dev. 85*, 3−14.
10. Tonks, N. K., Diltz, C. D., and Fischer, E. H. (1988) *J. Biol. Chem. 263*, 6722−6730.
11. Tonks, N. K., Diltz, C. D., and Fischer, E. H. (1988) *J. Biol. Chem. 263*, 6731−6737.
12. Charbonneau, H., Tonks, N. K., Walsh, K. A., and Fischer, E. H. (1988) *Proc. Natl. Acad. Sci. U.S.A. 85*, 7182−7186.
13. Chernoff, J., Schievella, A. R., Jost, C. A., Erikson, R. L., and Neel, B. G. (1990) *Proc. Natl. Acad. Sci. U.S.A. 87*, 2735−2739.
14. Hashimoto, N., Zhang, W. R., and Goldstein, B. J. (1992) *Biochem. J. 284*, 569−576.
15. Lammer, R., Bossenmaier, B., Cool, D. E., Tonks, N. K., Schlessinger, J., Fischer, E. H., and Ullrich, A. (1993) *J. Biol. Chem. 268*, 22456−22462.
16. Kenner, K. A., Anyanwu, E., Olefsky, J. M., and Kusari, J. (1996) *J. Biol. Chem. 271*, 19810−19816.
17. Seely, B. L., Staubs, P. A., Reichart, D. R., Perhanu, P., Milarski, K. L., Satiel, A. R., Kusari, J., and Olefsky, J. M. (1996) *Diabetes 45*, 1379−1385.
18. Liu, F., and Chernoff, J. (1997) *Biochem. J. 327*, 139−145.
19. Elchelby, M., Payette, P., Michaliszyn, E., Cromlish, W., Collins, S., Lee Loy, A., Normandin, D., Cheng, A., Himms-Hagen, J., Chan, C.-C., Ramachandran, C., Gresser, M. J., Tremblay, M. L., and Kennedy, B. P. (1999) *Science 283*, 1544−1548.
20. Frangioni, J. V., Beahm, P. H., Shifrin, V., Jost, C. A., and Neel, B. G. (1992) *Cell 68*, 545−560.
21. Woodford-Thomas, T. A., Rhodes, J. D., and Dixon, J. E. (1992) *J. Cell Biol. 117*, 401−414.
22. Pallen, C. J., Lai, D. S. Y., Chia, H. P., Boulet, I., and Tong, P. H. (1991) *Biochem. J. 276*, 315−323.
23. Cho, H., Ramer, S. E., Itoh, M., Winkler, D. G., Kitas, E., Bannwarth, W., Burn, P., Saito, H., and Walsh, C. T. (1991) *Biochemistry 30*, 6210−6216.
24. Cho, H., Krishnaraj, R., Itoh, M., Kitas, E., Bannwarth, W., Saito, H., and Walsh, C. T. (1993) *Protein Sci. 2*, 977−984.
25. Zhang, Z.-Y., Thieme-Sefler, A. M., Maclean, D., Roeske, R., and Dixon, J. E. (1993) *Anal. Biochem. 211*, 7−15.
26. Zhang, Z.-Y., Maclean, D., Thieme-Sefler, A. M., McNamara, D., Dobrusin, E. M., Sawyer, T. K., and Dixon, J. E. (1993) *Proc. Natl. Acad. Sci. U.S.A. 90*, 4446−4450.
27. Zhang, Z.-Y., Maclean, D., McNamara, D. J., Sawyer, T. K., and Dixon, J. E. (1994) *Biochemistry 33*, 2285−2290.
28. Hippen, K. L., Jakes, S., Richards, J., Jena, B. P., Beck, B. L., Tabatabai, L. B., and Ingebritsen, T. S. (1993) *Biochemistry 32*, 12405−12412.
29. Ruzzene, M., Donella-Deana, A., Marin, O., Perich, J. W., Ruzza, P., Borin, G., Calderan, A., and Pinna, L. A. (1993) *Eur. J. Biochem. 211*, 289−295.
30. Dechert, U., Affolter, M., Harder, K. W., Mathews, J., Owen, P., Clark-Lewis, I., Thomas, M. L., Aebersold, R., and Jirik, F. R. (1995) *Eur. J. Biochem. 231*, 673−681.
31. Wu, L., Buist, A., den Hertog, J., and Zhang, Z.-Y. (1997) *J. Biol. Chem. 272*, 6994−7002.
32. Zhang, Z.-Y., Walsh, A. B., Wu, L., McNamara, D. J., Dobrusin, E. M., and Miller, W. T. (1996) *J. Biol. Chem. 271*, 5386−5392.
33. Vetter, S. W., Keng, Y.-F., Lawrence, D. S., and Zhang, Z.-Y. (2000) *J. Biol. Chem. 275*, 2265−2268.
34. Jia, Z., Barford, D., Flint, A. J., and Tonks, N. K. (1995) *Science 268*, 1754−1758.
35. Puius, Y. A., Zhao, Y., Sullivan, M., Lawrence, D. S., Almo, S. C., and Zhang, Z.-Y. (1997) *Proc. Natl. Acad. Sci. U.S.A. 94*, 13420−13425.
36. Otwinowski, Z., and Minor, W. (1997) *Methods Enzymol. 276*, 307−326.
37. Kleywegt, G., and Jones, T. A. (1996) *Acta Crystallogr. D52*, 826−828.
38. Navaza, J., and Saludjian, P. (1997) *Methods Enzymol. 276*, 581−594.
39. Brünger, A. T. (1992) *X-PLOR Version 3.1: a System for Protein Crystallography and NMR*, Yale University Press, New Haven, CT.
40. Brünger, A. T., Adams, P. D., Clore, G. M., DeLano, W. L., Gros, P., Grosse-Kunstleve, R. W., Jiang, J.-S., Kuszewski, J., Nilges, N., Pannu, N. S., Read, R. J., Rice, L. M., Simonson, T., and Warren, G. L. (1998) *Acta Crystallogr. D54*, 905−921.
41. Jiang, J. S., and Brünger, A. T. (1994) *J. Mol. Biol. 243*, 100−115.
42. Jones, T. A., Zou, J. Y., Cowan, S. W., and Kjeldgaard, M. (1991) *Acta Crystallogr. A47*, 110−119.
43. Kleywegt, G., and Jones, T. A. (1997) *Methods Enzymol. 277*, 208−230.
44. Brünger, A. T. (1997) *Methods Enzymol. 277*, 366−396.
45. Laskowski, R. A., MacArthur, M. W., Moss, D. S., and Thornton, J. M. (1993) *J. Appl. Crystallogr. 26*, 283−291.
46. Vriend, G. (1990) *J. Mol. Graphics 8*, 52−56.
47. Glover, N. R., and Tracey, A. S. (1999) *Biochemistry 38*, 5256−5271.
48. Flint, A. J., Tiganis, T., Barford, D., and Tonks, N. K. (1997) *Proc. Natl. Acad. Sci. U.S.A. 94*, 1680−1685.
49. Huyer, G., Kelly, J., Moffat, J., Zamboni, R., Jia, Z., Gresser, M. J., and Ramachandran, C. (1998) *Anal. Biochem. 258*, 19−30.
50. Pellegrini, M. C., Liang, H., Mandiyan, S., Wang, K., Yuryev, A., Vlattas, I., Sytwu, T., Li, Y.-C., and Wennogle, L. P. (1998) *Biochemistry 37*, 15598−15606.
51. Evans, S. V. (1993) *J. Mol. Graphics 11*, 134−138.
52. Engh, R. A., and Huber, R. (1991) *Acta Crystallogr. A47*, 392−400.
53. Martin, A. C. R. (1995) *ProFit V1.6: Protein Least Squares Fitting*, SciTech Software, Ashtead, Surrey, U.K.
54. Barford, D., Flint, A. J., and Tonks, N. K. (1994) *Science 263*, 1397−1404.
55. Stuckey, J. A., Fauman, E. B., Schubert, H. L., Zhang, Z.-Y., Dixon, J. E., and Saper, M. A. (1994) *Nature 370*, 571−575.
56. Wallace, A. C., Laskowski, R. A., and Thornton, J. M. (1995) *Protein Eng. 8*, 127−134.
57. Sarmiento, M., Zhao, Y., Gordon, S. J., and Zhang, Z.-Y. (1998) *J. Biol. Chem. 273*, 26368−26374.

BI000319W